Intraoperative functional remapping unveils evolving patterns of cortical plasticity

Sam Ng, Pablo Valdes, Sylvie Moritz-Gasser, Anne-Laure Lemaitre, Hugues Duffau, Guillaume Herbet

Intraoperative functional remapping unveils evolving patterns of cortical plasticity

Sam Ng,[1,2,†] Pablo A. Valdes,[3,†] Sylvie Moritz-Gasser,[1,2] Anne-Laure Lemaitre,[1,2] Hugues Duffau[1,2] and Guillaume Herbet[1,2,4]

[†]**These authors contributed equally to this work.**

Abstract

The efficiency with which the brain reorganizes following injury not only depends on the extent and the severity of the lesion, but also on its temporal features. It is established that diffuse low-grade gliomas (DLGG), brain tumours with a slow-growth rate, induce a compensatory modulation of the anatomo-functional architecture, making this kind of tumours an ideal lesion model to study the dynamics of neuroplasticity. Direct electrostimulation (DES) mapping is a well-tried procedure used during awake resection surgeries to identify and spare cortical epicenters which are critical for a range of functions. Because DLGG is a chronic disease, it inevitably relapses years after the initial surgery, and thus requires a second surgery to reduce tumour volume again. In this context, contrasting the cortical mappings obtained during two sequential neurosurgeries offers a unique opportunity to both identify and characterize the dynamic (*i.e.* re-evolving) patterns of cortical re-arrangements.

Here, we capitalized on an unprecedented series of 101 DLGG patients who benefited from two DES-guided neurosurgeries usually spaced several years apart, resulting in a large DES dataset of 2082 cortical sites. All sites (either non-functional or associated with language, speech, motor, somatosensory and semantic processing) were recorded in the Montreal Neurological Institute (MNI) space. Next, we used a multi-step approach to generate probabilistic neuroplasticity maps that reflected the dynamic rearrangements of cortical mappings from one surgery to another, both at the population and individual-level.

Voxel-wise neuroplasticity maps revealed regions with a relatively high potential of evolving reorganizations at the population level, including the supplementary motor area (SMA, p_{max} = 0.63), the dorsolateral prefrontal cortex (dlPFC, p_{max} = 0.61), the anterior ventral premotor cortex (vPMC, p_{max}=0.43) and the middle superior temporal gyrus (STG p_{max}= 0.36). Parcel-wise neuroplasticity maps confirmed this potential for the dlPFC (Fisher's exact test, $p_{FDR\text{-}corrected} = 6.6^{e\text{-}5}$), the anterior ($p_{FDR\text{-}corrected}$ = 0.0039) and the ventral precentral gyrus ($p_{FDR\text{-}corrected}$

= 0.0058). A series of clustering analyses revealed a topological migration of clusters, especially within the left dlPFC and STG (language sites); the left vPMC (speech arrest/dysarthria sites) and the right SMA (negative motor response sites). At the individual level, these dynamic changes were confirmed for the dlPFC (bilateral), the left vPMC and the anterior left STG (threshold free cluster enhancement, 5000 permutations, family-wise-error-corrected).

Taken as a whole, our results provide a critical insight into the dynamic potential of DLGG-induced continuing rearrangements of the cerebral cortex, with considerable implications for re-operations.

Author affiliations:

1 Department of Neurosurgery, Gui de Chauliac hospital, Montpellier University Medical Center, Montpellier, France

2 Institute of Functional Genomics, University of Montpellier, CNRS, INSERM, Montpellier, France

3 Department of Neurosurgery, University of Texas Medical Branch, Galveston, Texas, USA

4 Praxiling laboratory, UMR 5267, CNRS, UPVM, Montpellier, France

Correspondence to: Guillaume Herbet

Bâtiment Marc Bloch (BRED) Université Paul-Valéry, Route de Mende, 34199 Montpellier cedex, France

E-mail: guillaume.herbet@umontpellier.fr

Running title: Cortical remodelling in recurrent gliomas

Keywords: plasticity; recurrent glioma; direct electrostimulation mapping; awake surgery; cognitive mapping; cortical rearrangement

Introduction

Neuroplasticity refers to the unique capacity of the brain to adapt its networks in response to experience or cognitive demands to maintain an optimal level of interactions with the ever-evolving internal or external environment.[1,2] Neuroplasticity can occur at multiple spatiotemporal scales, from fast remodelling of neurosynaptic maps to long-term rewiring of long-range white matter connections.[3] From a behavioural standpoint, this neural malleability is mirrored in the human's capacity to learn an impressive array of new skills and to produce creative behaviours. For example, it is established that acquiring a new language[4] or learning a new musical instrument[5] causes measurable structural and functional brain variations.[6]

In the pathophysiological domain, neuroplasticity refers to the brain's ability to reorganize following structural damage (*e.g.* stroke, tumour, traumatic brain injury) in an attempt to maintain or re-establish normal function. Postlesional neuroplasticity has been the subject of numerous studies, especially in the context of acute lesions such as stroke or traumatic brain injury, with the objective of identifying the different strategies that the brain deploys to compensate for neuronal losses and the factors predictive of functional recovery.[7–9] Over different lesion models, diffuse low-grade gliomas (WHO grade II diffuse glioma[10], DLGG), a subgroup of primary brain tumours with a slow-growth rate, have been highlighted as an exemplary model for studying neuroplasticity.[11,12] At the cellular level, the dynamic interplay between glioma cells and their local microenvironment results in complex electrical and synaptic integration into neural circuits[13,14] that promotes long-range modulations of neural signalling and activities.[15] At the macroscale level, there is increasing evidence that the slow-growth kinetics of DLGG favour a dynamic network re-organization,[16–18] whose mechanistic principles remain to be characterised. These whole brain neuroplastic modulations may account for the common but remarkable observation that cognitive impairments in DLGG patients are relatively low both before and after neurosurgery,[19] despite sometimes large resections of cortical areas ordinarily considered as "eloquent".[20]

As DLGG is a chronic disease, it will inevitably relapse years or even decades after the initial resection, requiring a second surgery to be performed in an attempt to again reduce tumour volume and prevent malignant transformation.[21,22] Currently, wide-awake surgery assisted with direct electrostimulation (DES) mapping is the gold standard treatment at diagnosis, as it has been shown to enhance both the extent of resection and life expectancy while drastically decreasing the likelihood of postoperative permanent, debilitating

neurological and neuropsychological deficits.[19,23] DES mapping is increasingly used at the time of reoperation in the event of DLGG recurrence, as it allows surgical resection to be extended beyond the functional limits identified with DES mapping during the first surgery.[24–26] The observation that reoperations are possible supports the hypothesis whereby tumour-induced plasticity may continue in a constant-evolving manner, in a co-dependent manner with tumour expansion, resulting in evolving patterns of cortical rearrangements.[12] In this context, contrasting the cortical mappings obtained between two sequential surgeries offers a unique opportunity to characterise the dynamics of cortical reorganisation and to identify the anatomic factors that constrain them.

Here, we took advantage of a unique DES cortical mapping dataset (2082 exploitable stimulation sites) gained from a cohort of 101 patients having undergone two distinct awake surgical procedures usually spaced several years apart. In contrast to alternate methods that can be used to study the dynamics of neuroplasticity, DES offers the clear advantage of causally linking human behaviors and neuroanatomy with a high reproducibility and spatiotemporal resolution.[27–29]

The main objectives of this study were threefold: (i) to investigate the potential of cortical structures to functionally evolve and remodel from one surgery to another under the form of gradients (from lowest to highest potential); (ii) to categorize the topological features of cortical rearrangements as a result of functional responses; (iii) to provide clinically relevant maps that account for the evolving capability of cortical structures to compensate over time.

Materials and methods

Study population

Data processed in this study were obtained in a clinical context and the procedures detailed below follow our standard clinical approach. All patients gave informed consent. Approval for the study was granted by the Institution Review Board of Montpellier University Medical Center (No.202000557).

The population screened for inclusion included all patients operated in our institution by a single surgeon (H.D.) between 2007 and 2021. The inclusion criteria were: (1) a diagnosis of DLGG, confirmed by histopathological and/or molecular analysis, (2) two surgical procedures spaced at least 6 months apart, (3) the use of cortical DES mapping under awake

conditions in both procedures. Intraoperative reports, photographs, camera recordings and neuroimaging data were consecutively collected and subjected to a retrospective analysis. Of note, only patients who remained free of radiation therapy (a treatment that may diminish the propensity for neuroplastic reorganization)[30] were included in the study.

In vivo electrostimulation procedure and behavioural paradigms

The surgical procedure was extensively described elsewhere[31,32] and the technique remained unchanged from Surg.1 to Surg.2. Briefly, patients systematically underwent an asleep-awake-asleep procedure. DES cortical mapping was performed during the awake phase, after craniotomy and dura (re-)opening. Electrical mapping was performed with a bipolar probe (inter-tip spacing: 5mm, NIMBUS stimulator, Newmedic, France) delivering a biphasic current (1ms pulse width, 60Hz, amplitude from 1.50mA to 3.50mA). DES never exceeded 4s to limit electrical spreading and to maintain anatomo-functional specificity. The amplitude was gradually increased up until functional responses (*i.e.*, transient speech disorders) were elicited within the ventral premotor cortex (vPMc). Then, the same amplitude was maintained constant during the whole procedure. Cortical sites were considered as positive ones if they elicited an inability to perform at least one of the intraoperative tasks within the 4s time delay, in a reproducible way, during at least three non-consecutive stimulations (see Figure 1A). Cortical sites that did not fulfil the criteria for a positive response were considered as negative ones. After completion of DES cortical mapping, the tumour removal was performed using subpial dissection. The resection was achieved until DES subcortical responses were obtained (following the principle of functionally guided tumour removal).[29]

Intraoperative tasks included upper limb movements, number counting (1-10), a picture naming task, a non-verbal semantic association task when tumours involved the right hemisphere (Pyramids and Palm Trees test).[33,34] Other cognitive tasks (e.g., line bisection task) were occasionally used[35–37] depending on the location of the tumour and the date of the surgery but were not considered in this study. Intraoperative cognitive monitoring was performed by a senior speech therapist (S.M.G.) or neuropsychologist (A.L.L., G.H.) who remained blind to the application of DES during the procedure. Note that each task was administered before surgery in order to decrease the likelihood of false positive responses during intraoperative mapping. The neuropsychologist and/or speech therapist checked whether movement disorders

were due to contraction/inhibition during each task (or dual tasking). This assessment was performed systematically for the face and the upper limbs.

The following positive (*i.e.* functional) responses were considered: (1) language impairments (including anomia and paraphasia), (2) speech disorders (including speech arrest and dysarthria), (3) negative motor responses of the upper limb, (4) positive motor responses of the face and upper limb, (5) dysesthesia and (6) semantic association disorders.

The above-mentioned intraoperative manifestations were determined as follows: a negative motor response was defined as a complete inhibition of movement without the loss of muscle tone or consciousness;[38,39] a positive motor response was defined as the contraction of a muscle or muscle group causing an involuntary movement;[40] speech arrest was defined as a complete discontinuation of the ongoing number counting or continuous speaking, without oral, facial, jaw, or tongue positive movements[32,39] (of note, it was not possible to perform a concomitant movement task of the face and thus to strictly distinguish a facial negative motor response from a speech arrest); anomia was defined as an inability to name an object, while still being able to pronounce the words "this is a [picture]" (naming task)[41], thus allowing to rule out a speech arrest manifestation; paraphasia was specifically defined by a misnaming of an object, using the same paradigm; dysarthria was defined as a disorder of articulatory planning and/or speech sound production (word groping, sound distortion, prosodic abnormalities), without oral, facial, jaw, or tongue positive movements; a semantic association disorder was defined as in incorrect response or an inability to respond during the Pyramid and Palm Tree task.

Functional responses in one of these categories at Surg.1 were only considered if the same task(s) were applied at Surg.2. Note that some stimulations could produce concomitant disorders and were further considered in both disorder categories in further analyses (*e.g.*, speech arrest plus negative motor response of the upper limb). Two photographs were done: one at the end of the cortical mapping, and one at the end of the resection. In addition, procedures were recorded with a built-in camera attached to the operating lights.

Neuroimaging processing

T1-weighted and fluid-attenuated inversion recovery (FLAIR) preoperative and postoperative MRI were systematically acquired the day before and at 3-months after both surgeries. MRIs were co-register to the Montreal Neurological Institute (MNI) space using enantiomorphic

normalization[42] with SPM12 (Statistical Parametric Mapping, https://www.fil.ion.ucl.ac.uk/spm/software/spm12) and the Clinical toolbox (https://www.nitrc.org/projects/clinicaltbx") implemented in MATLAB environment (Release 2018a, The MathWorks Inc., Natick, NA, USA).

Spatial positioning of DES sites

The MNI coordinates for each stimulation site were determined after inspection of operative reports, intraoperative photographs (positive stimulations) and intraoperative videos (negative sites), as illustrated in Figure 1B and 1C. This method was previously demonstrated to provide an high inter-observer reliability.[27,43] The MRI obtained 3 months after Surg.1 was systematically used as the reference image for spatial positioning, since it allowed a comparison between the post-resection photograph obtained during Surg.1 and the pre-resection photograph obtained during Surg.2. In addition, 3-dimensional pial-mesh reconstructions of the MRI obtained 3 months after Surg.1 were generated with BrainVISA/Anatomist software (Version 5.0, CEA I2BM, CATI Neuroimaging, Inserm IFR49, and CNRS, France) to allow a 3D visualization of individual cortical structures and a semi-automated MNI coordinate-surface matching of the model (Figure 1D). To demonstrate the reproducibility of the procedure used to position cortical sites despite a more challenging identification of gyro-sulcal anatomy at reoperation,[44] intra- and inter-observer correlation coefficients were computed. More specifically, the first observer positioned two times consecutively 100 stimulation sites randomly selected within the left hemisphere. Pearson correlations were performed between each set of coordinates to derive measures of intra-observer agreement (one for each axis). Likewise, a second observer also positioned the same 100 sites to derive this time measures of inter-observer agreement. We also used simple two-tailed *t*-tests to check for differences between each coordinate dataset. Note that the procedure was performed by two experts in neuroanatomy. Overall, we found a high degree of intra and inter-observer agreement (see Supplementary Figure 1).

Probabilistic distributions of functional sites

Voxel-wise density maps

For each DES site, we assumed that the associated functional response f_i (where i corresponds to a given stimulation with $i=1,\ldots, n$ for n stimulations) is maximal at the centre of the stimulated area. Furthermore, to account for the spread of the electrical current nearby this central position, we approximated f_i in all surrounding voxels (from 1 at the centre to 0 in all voxels sufficiently distant from this centre) with a standard kernel regression technique. Using the function "fslmaths" in FMRIB Software Library program (FSL, version 6.0, https://fsl.fmrib.ox.ac.uk/fsl), we applied a full width at half maximum (FWHM) of 8mm (bandwidth ≈3.4mm) for each DES site, which is more conservative than previous studies pointing out that bandwidth values were acceptable until 4-5mm in the same experimental settings.[28,45] In order to represent the spatial distribution of all stimulation sites, we then computed a voxel-wise overlap map by summing individual kernel-transformed maps. Consequently, for each voxel x of the brain, we obtained a density overlap map with $\text{Density}_x = \sum_{i=1}^{n} f_i$

Voxel-wise probability maps

To map the potential of cortical areas to be associated with positive or negative responses, we computed voxel-wise probability maps by calculating the ratio of positive responses and negative responses in each voxel. In particular, we defined the probability that a given voxel x of the brain is implicated in a functional response as a positive probability, and the probability that a given voxel x of the brain is implicated in a negative response as a negative probability. Thus, we calculated positive and negative probability maps at Surg.1 and Surg.2 with the following formula:

$$Positive\_Probability_x = \sum_{i=1}^{v} f\_positive_i / \left(\sum_{i=1}^{v} f\_positive_i + \sum_{k=1}^{w} f\_negative_k\right)$$

$$Negative\_Probability_x = \sum_{k=1}^{w} f\_negative_k / \left(\sum_{i=1}^{v} f\_positive_i + \sum_{k=1}^{w} f\_negative_k\right)$$

where $f\_positive_i$ and $f\_negative_j$ are the functional responses of v positive stimulation(s) (with $i=1,\ldots,v$) and w negative stimulation(s) (with $k=1,\ldots,w$).

Voxel-wise plastic probability maps

To capture the propensity of cortical areas to be functional at Surg.1, while becoming non-functional at Surg.2, which can be interpreted as a marker of cortical remodelling, we further computed a probability map representing the intersection between positive probability maps at Surg.1 and negative probability maps at Surg.2 as follows (*i.e.* a plasticity probability map):

$Plasticity\_Probability_x = Surg.1\_positive\_probability_x * Surg.2\_negative\_probability_x$

Parcel-wise probability map

Next, we used predefined cortical parcels to contextualize the ratio between positive and negative responses in terms of anatomical location. Our goal was to allow an explicit assignment of DES effects in specific anatomical structures. This approach also permits a substantial reduction of the dimensionality of the stimulation dataset in comparison to voxel-based analyses. To estimate the probability of obtaining a positive response within *a priori* anatomical parcellations, we used the Brainnetome atlas (https://atlas.brainnetome.org/bntatlas, composed of 123 labelled parcels, see Supplementary materials for a list of all cortical parcels). More specifically, we divided the number of positive DES by the total number of DES (positive and negative) in a given parcel. For instance, the probability of observing a positive response during Surg.1 within the region 6_1 of the left Precentral gyrus (left PrG_6_1) was 0.973 (*i.e.*, 215 positive DES/ 221 positive and negative DES). Each stimulation site was generated as an MNI-registered sphere using Marsbar Toolbox (radius=5mm), implemented in the MATLAB environment (https://marsbar-toolbox.github.io). To determine the location of each sphere in terms of anatomical parcels, we used the Lesion Quantification Toolkit (https://wustl.app.box.com/v/LesionQuantificationToolkit)[46]. The function "util_get_parcel_damage" was applied for each stimulation point (see Supplementary Figure 2 and Supplementary materials for more details and links to custom MATLAB codes). The ratio of positive and negative DES was then compared between Surg.1 and Surg.2, within each anatomical parcel with >3 DES, using Fisher's exact tests. Benjamini-Hochberg's false discovery rate (FDR) correction for multiple comparisons was used in each hemisphere separately, with a threshold set at $P < 0.05$ (*Rstudio*, 2021.09.1 Build 372, www.r-project.org).

Clustering analyses

K-mean clustering

Clustering analyses were performed to assess the extent to which the distribution pattern of functional sites was changing from Surg.1 to Surg.2. In this analysis, only positive stimulations were considered. Clustering analyses were performed separately at Surg.1 and Surg.2. For a given behaviour response of interest (*i.e.* language disorders, speech arrest and dysarthria, positive motor responses and negative motor responses), the MNI coordinates of all stimulation sites were analysed with *R* software using the Flexible Procedures for Clustering package (fpc, version 2.2-9). Note that somatosensorial responses were not considered here, because of the limited amount of available data per hemisphere during Surg.2. A Duda-Hart statistic was used to determine whether a given dataset should be clustered. Datasets with a Duda-Hart statistic >1.645 were further subjected to a *k*-mean clustering; the remaining ones were represented as single clusters. The optimal number of clusters (range: 2-10) was determined using the most conservative result (*i.e.* the smallest number of suggested clusters) obtained from the average silhouette width method and the Calinski Harabasz index method. Stimulation sites and their related centroids were further plotted in a z/y MNI graph representation to allow an easier visualization of their locations.

Cluster comparisons

Based on a qualitative analysis, we next identified: (i) Clusters presenting with spatial similarities but potential shifts of their coordinates from Surg.1 to Surg.2. To provide a quantitative overview of cluster shifts, the MNI coordinates of stimulations sites forming similar clusters were analysed with two-tailed *t*-tests. FDR correction for multiple comparisons was used for each hemisphere separately, with a threshold set at $P < 0.05$; (ii) Clusters that disappeared from Surg.1 to Surg.2 and their related centroids; (iii) Clusters that appeared from Surg.1 to Surg.2 and their related centroids.

Dynamic remodelling of individual functional cortical maps

Individual functional cortical maps

To better highlight the neuroplasticity potential outlined in previous analyses, we directly contrasted the changes in the distribution of functional responses from one surgery to another at the individual level. First, we identified cortical areas that were uniformly covered by DES from one surgery to another in each patient by generating a reference binarized map

corresponding to the intersection map between the sum of all stimulations at Surg.1 and Surg.2. By doing so, areas eliciting positive (or negative) response during only one of the two electrostimulation sessions were not considered in further statistical analyses.

Second, we computed an individual functional cortical map accounting for positive responses at Surg.1 and Surg.2 in each patient. Briefly, we computed functional responses in each patient using a standard kernel regression technique to approximate a cortical functional map (with each voxel having a value between 0 and 1) exclusively within the previously generated intersection map (*i.e.* within voxels covered by DES during both Surg.1 and Surg.2).

Individual functional cortical maps were computed to investigate plasticity in general (*i.e.* all positive functional responses were selected), or in the different functional responses taken separately. It should be mentioned that non-responsive DES sites for a given function of interest were considered as non-functional DES (*e.g.* in language mapping, DES eliciting positive motor responses without associated language disorders were considered negative for language). More details and links to custom MATLAB codes are provided in Supplementary figure 3 and Supplementary materials).

Surg.1 and Surg.2 statistical comparisons

Each patient's functional cortical maps (FCMs) at Surg.1 and Surg.2 were then used to study the cortical neuroplastic changes from one surgery to another. To do so, non-parametric statistics were performed, using the "randomise" function from FSL with 5000 permutations and threshold free cluster enhancement. To achieve a paired comparison analysis, we calculated the difference between Surg.1 and Surg.2 FCMs within-subjects ($FCM_{Surg.1}$ - FCMSurg.2, using "fslmaths" function) and then performed a one sample *t*-test across subjects, which is equivalent to a paired *t*-test (https://fsl.fmrib.ox.ac.uk/fsl/fslwiki/Randomise/UserGuide). We corrected for multiple comparisons with a family-wise error (FWE) threshold set at $P < 0.05$. Since we assumed a prior hypothesis that individual FCMs were more restricted at Surg.2 compared to Surg.1 ($FCM_{Surg.1}$-$FCM_{Surg.2}$>0) due to higher neuroplastic compensations, we only provide the results of one sample t-tests. Of note, we also performed the same analysis with the opposite contrast (difference between Surg.2 and Surg1.) but found no significant results.

To mitigate the potential effect of clinical or biological factors that may modulate cortical plasticity, we next repeated the same analysis using 'stimulation intensity changes from Surg.1 to Surg.2', 'histomolecular classification', 'the use of chemotherapy between Surg.1 and

Surg.2' and the 'time interval between Surg.1 and Surg.2' as nuisance covariates. Briefly, we independently tested the effect of these covariates with both a 1/0 and a 0/1 contrasts within the corresponding design matrix (FEAT interface, https://fsl.fmrib.ox.ac.uk/fsl/fslwiki/GLM) before running "randomise" function from FSL.

Residual functional cortical map, regrowth functional cortical map and extra-lesional functional cortical map

To assess whether the spatial patterns of tumour regrowth modulated cortical plasticity, we next confronted the individual FCMs to each patient's tumoral infiltration pattern, based on FLAIR images obtained 3 months after Surg.1 and immediately before Surg.2. As a result, in each patient we were able to discriminate (1) a residual functional cortical map (changes of FCM only within post-Surg.1 tumour residual), (2) a regrowth functional cortical map (changes of FCM only within changes of FLAIR signal observed between post-Surg.1 and pre-Surg.2 MRIs) and (3) an extra-lesional functional cortical map (changes of FCM only outside pre-Surg.2 tumour signal). Non-parametric statistics were then performed to compare each patient's FCM, using the "randomise" function from FSL with 5000 permutations and threshold free cluster enhancement (see above). Methodological details are illustrated in **Supplementary Figure 4**.

Data availability

Data will be made available upon reasonable request to the corresponding author.

Exhaustive datasets are provided in the Supplementary materials, including custom MATLAB codes. Visualization of the results were made with MRIcroGL (https://www.nitrc.org/projects/mricrogl) and SurfIce (https://www.nitrc.org/projects/surfice).

Results

Participants

Overall, 101 patients underwent repeat awake-guided surgical resections for a DLGG (49 female [48.5%], mean age at first surgery: 34.5 ± 9.1). Details about mean tumour volumes before/after surgeries and the extent of resections are provided in the Supplementary materials.

Pre-surgical, post-surgical and tumour regrowth infiltration maps are displayed in Supplementary Figure 5. The mean time interval between Surg.1 and Surg.2 was 53.52 ± 27.59 months (range: 7-125 months). Histopathological features at Surg.1 and Surg.2 are detailed in the Supplementary materials. Note that 3 patients had a change of histomolecular classification from Surg.1 to Surg.2 due to the absence of 1p19q codeletion and/or IDH1/2 mutation at the first surgery. In addition, 13 patients (12.9%) presented with a change of grade according to the WHO classification at Surg.2. Details about seizure control and the use of antiepileptic drugs before Surg.1/Surg.2 are reported in the Supplementary materials. No patients received radiation therapy before Surg.2. Thirty patients (29.7%) received chemotherapy between Surg.1 and Surg.2 (Temolozomide alone: 24 patients; Procarbazine/Lomustine/Vincristine: 3 patients; a combination of both at different time points: 3 patients).

The total number of eligible cortical DES was 2082, including 1291 during Surg.1 (485 positive stimulations, 806 negative stimulations) and 791 during Surg.2 (351 positive stimulations, 440 negative stimulations). The mean DES amplitude was 2.31 ± 0. 58 mA. There were no significant changes of stimulation intensities from Surg.1 to Surg.2 (mean intensity at Surg1: 2.29 ± 0.60 mA, mean intensity at Surg2: 2.33 ± 0.56 mA, two-tailed paired t-test: $t_{(100)} = 0.64$, $p = 0.52$). The locations of all stimulation sites are displayed in Figure 1E and 1F. Among positive stimulations, 91 elicited language disorders (45 during Surg.1 and 46 during Surg.2), 406 elicited speech production disorders (237 during Surg.1 and 169 during Surg.2), 164 elicited negative motor responses (65 during Surg.1 and 99 during surg.2), 230 elicited positive motor responses (134 during Surg.1 and 96 during Surg.2), 73 elicited somatosensory disorders (52 during Surg.1 and 21 during Surg.2) and 38 elicited semantic association disorders (19 during Surg.1 and 19 during Surg.2, all within the right hemisphere).

Probability maps

Voxel-wise probability maps

Density maps and left and right voxel-wise positive probability maps are displayed in Figure 2A. Additional negative density maps are detailed in Supplementary figure 6. Voxel-wise

probabilistic neuroplasticity maps are displayed in Figure 2B. The maximal probabilities p_{max} (from 0, lowest neuroplasticity, to 1, highest neuroplasticity) were observed within the right SMA (p_{max} = 0.63), the right dlPFC (p_{max} = 0.61), the left supramarginalis gyrus (SMG, p_{max}= 0.49), the left anterior part of the ventral PMC (p_{max} = 0.43), the left dlPFC (p_{max} = 0.39) and the middle portion of the left STG (STG, p_{max} = 0.36).

Parcel-wise probability maps

Parcel-wise probabilistic maps and related significant statistical comparisons are illustrated in Figure 2C-F. The number of stimulations (positive and negative) in each parcel is detailed in Supplementary materials.

The analyses indicated significant changes in probability distributions between positive and negative DES in the following parcels: left PrG6_1 parcel (*Fisher's exact test*, $p_{FDR\text{-}corrected}$ = $2.6^{e\text{-}5}$) the left PrG6_2 ($p_{FDR\text{-}corrected}$ = 0.046), the left PrG6_6 ($p_{FDR\text{-}corrected}$ = 0.046), the right MFG7_2 ($p_{FDR\text{-}corrected}$ = $6.6^{e\text{-}5}$), the right PrG6_1 ($p_{FDR\text{-}corrected}$ = 0.0058) and the right PrG6_6 ($p_{FDR\text{-}corrected}$ = 0.0039). In all above-mentioned parcels, the ratio of positive/negative stimulations consistently decreased at Surg.2, with the exception of the left supramarginal gyrus (left IPL6_4, $p_{FDR\text{-}corrected}$ = 0.046).

Clustering analyses

Clustering analysis results, locations of cluster centroids and significant shifts of cluster MNI coordinates between Surg.1 and Surg.2 are provided in Figure 3.

Within the left hemisphere, significant cluster migrations were found for language responses ($n_{Surg.1}$ = 45 stimulations [4 clusters], $n_{Surg.2}$ = 46 stimulations [3 clusters], see Figure 3A), with a significant antero-posterior shift of paired centroids within the dlPFC (mean MNI_y-coordinates change = -10.4 ± 3.0 $t_{(32)}$ = 3.46, $p_{\text{FDR-corrected}}$ = 0.007). In addition, a language cluster located within the left STG during Surg.1 (centroid MNI coordinates [-65.1; -22.3; 7.7]) disappeared at Surg.2. Cluster shifts were also found in speech arrest/dysarthria ($n_{Surg.1}$ = 167 stimulations [2 clusters], $n_{Surg.2}$ = 115 stimulations [2 clusters], see Figure 3C) with a ventro-dorsal shift of a cluster located within the medio-dorsal part of the precentral gyrus (mean MNI_x-coordinates change = 8.3 ± 2.0, $t_{(87)}$ = 4.23 $p_{\text{FDR-corrected}}$ < 0.0001; mean MNI_z-coordinates change = 9.1 ± 2.0, *t(87)* = 4.49, $p_{\text{FDR-corrected}}$ < 0.0001). An additional cluster was identified at Surg.2 regarding stimulations eliciting negative motor responses (left precentral gyrus, centroid

MNI coordinates [-35.9; -5.6; 61.6], see Figure 3E). No cluster change was observed for stimulations provoking positive motor responses (Figure 3G).

Within the right hemisphere, cluster locations were also comparable regarding DES-induced non-verbal semantic disorders ($n_{Surg.1}$ = 9 stimulations [1 cluster], $n_{Surg.2}$ = 12 stimulations [1 cluster], see Figure 3B). Additional clusters were identified at Surg.2, especially regarding stimulations eliciting speech arrest/dysarthria (right SMG, centroid MNI coordinates [64.2; -24; 32], see Figure 3D) and negative motor responses (right precentral gyrus, centroid MNI coordinates [49.6; 0.88; 50.7], see Figure 3F). Interestingly an antero-posterior shift of a cluster located within the right upper precentral gyrus/right SMA toward the right upper precentral gyrus was observed (mean MNI_y-coordinates change = -13.8 ± 3.0, $t_{(28)} = 4.55$, $p_{FDR\text{-}corrected} < 0.0001$, Figure 3F). No significant changes in cluster coordinate positioning were observed between the two surgeries for stimulations provoking positive motor responses within the right hemisphere ($n_{Surg.1}$ = 64 stimulations [2 clusters], $n_{Surg.2}$ = 54 stimulations [2 clusters], see Figure 3H).

Dynamic reorganizations of individual functional cortical maps

The overlap of cortical areas being stimulated both at Surg.1 and Surg.2 at the individual level is displayed in Figure 4A. Statistically significant differences between both functional cortical maps are provided as 1-*p* maps (FWE-corrected, threshold free cluster enhancement, 5000 permutations). The results of FCM comparisons when adjusted for each covariate independently (*i.e.* stimulation intensity changes, histomolecular classification, the use of chemotherapy and the time interval between Surg.1 and Surg.2) still remained significant, with only modulations in terms of cluster size. In addition, no linear significant relationships were observed between FCM measures and each covariate taken separately (see Supplementary Materials). Results by behavioural response (Figure 4B) indicate significant reorganizations (i) for language responses within both the left dlPFC and the left anterior STG, (ii) for speech arrest/dysarthria within the left vPMC and to some extent at the junction between the right dorsal PMC and the precentral gyrus (iii) for semantic response within the right dlPFC and (iv) for negative motor responses within the right vPMC. Cortical areas eliciting positive motor responses (left and right hemispheres) and negative motor responses (left hemisphere) remained unchanged from Surg.1 to Surg.2. Overall, high neuroplastic reorganizations occurred in the

left dlPFC, the left vPMC, the posterior part of the inferior frontal gyrus (IFG), the anterior part of the left STG and the right dlPFC (Figure 4C).

Significant voxels were found both within the residual functional cortical map, the regrowth functional cortical map and the extra-lesional functional cortical map, highlighting cortical plasticity potential both within and directly around the cortical tumoral infiltration (see Supplementary Figure 7).

Discussion

The unique ability of the cerebral cortex to rearrange the topological organization of its cortical networks has been highlighted in response to various pathological settings, including peripheral lesions (*e.g.* in case of depravation of normal sensory inputs),[2,47] congenital or brain injuries such as brain tumours and stroke.[48,49] It is widely acknowledged that lesion-induced plasticity is a time-dependent process, though it has been rarely investigated longitudinally, especially in the context of slow-growing tumours where neuroplastic changes are widespread. In other words, the longitudinal study of DLGG patients may help address fundamental questions about the properties of tumour-induced plasticity: Is postlesional plasticity a time-limited process? Is the potential for cortical remodelling equivalent across brain areas?

In the present study, we capitalized on a large and longitudinal electrostimulation dataset acquired from patients with DLGG to test the hypothesis that lesion-induced plasticity follows an evolving and spatially constrained scheme across the human cortex. Overall, our results show that (i) cortical areas have a potential for evolving rearrangements which is however graded across the cortex; (ii) this dynamic potential appears to be constrained by the underlying functional neuroanatomy (*e.g.*, primary sensorimotor cortices) and (iii) the efficiency of cortical rearrangements might be domain-specific, with higher plastic potentials in cortical circuits underpinning language and speech production.

The temporal pattern of tumour expansion is believed to be a key mechanistic principle governing the efficiency with which neuroplasticity deploys in DLGG patients.[16] However, there is only a handful of studies that have investigated the longitudinal features of glioma-induced neuroplasticity in general[50,51] – those using DES mapping being based on small datasets.[24,25] Here we showed that the potential of cortical areas to undergo glioma-induced rearrangement evolves from one surgery to another, albeit with an important variability across

the cerebral cortex. Furthermore, we demonstrated that cortical plasticity evolves not only within the lesion, but also around the cortical infiltration. This confirms that important spatial cortical rearrangements occur as a consequence of a dynamic interplay between the brain and the tumour, as reported in previous case series.[25,52] In addition, the present study suggests a marked heterogeneity in the plasticity potential across cortical structures. Such differing potential can be conceived as a gradient, the value of which varies as a function of cortical areas. Low gradients of plasticity were mainly found within unimodal cortical structures, those which belong to what have been previously called the "minimal common brain" (*i.e.* a universal trunk formed by cortico-subcortical structures that is essential for basic cerebral functions, with low interindividual variability),[53] including the primary somatosensory and motor cortices. This result aligns with that of a recent MEG study showing only subtle ipsilesional longitudinal changes of motor activations in patients with recurrent gliomas.[50] Admittedly however, the restricted plasticity potential observed in the primary motor areas at reoperation has to be interpreted in the light of a limited tumoral regrowth within cortical areas of the precentral gyrus (in particular, the primary hand area), while adjacent connective tracts were generally more infiltrated compared to the initial surgery. Increasing sample size in future studies may help capture a more in-depth picture of the potential of all cortical motor areas to be rewired following glioma relapse, an important point considering that plasticity of the primary sensorimotor cortex at first operation has been sometimes described.[52,54–56]

Remarkably, cluster analyses confirmed that positive language sites within the middle portion of the STG tended to turn negative during the second surgery, thus supporting the results of a recent MEG study indicating that the neural network underpinning language may be especially plastic in recurrent glioma patients, the mechanism of which would be a laterality shift in hemispheric specialization.[51]

Interestingly, we observed higher gradients of neuroplasticity within the vPMC, a result that was not particularly expected given the role of this region in speech production and its topologically-constrained neuroplasticity potential at initial surgery.[57] Indeed, the speech-related lateral part of the precentral gyrus was substantially rearranged between two surgeries, with a migration of sites from the ventral to the dorsal premotor cortex. This intragyral reorganisation may be explained by the fact that the third branch of the superior longitudinal fasciculus, which is known to convey speech articulatory related information from the supramarginal gyrus to the vPMC,[58] also projects more dorsally in the precentral gyrus. In other words, one can speculate that the dorsal trajectory of cortical rearrangements might depend on

the connective properties of the superior longitudinal fasciculus III. Likewise, the high potential for evolving neuroplastic compensation within the posterior dlPFC appears to be challenging given its topological positioning into the anatomo-functional architecture. Indeed, the dlPFC acts as a high-centrality cortical hub, and is thought to support transmodal integration.[59] Yet, our findings might be sustained by further functional compensation within the contralateral dlPFC, given the expected contribution of both dlPFC especially in semantic processing.[33]

Our results may have important clinical implications in at least two directions. First, DLGG are diffuse neoplasms showing a recurrent infiltration within the brain parenchyma. In the context of multistage surgical management,[60] a better understanding of the mechanistic principles of cortical reallocation over time is of major importance to assess re-operability in patients for whom the glioma recurs (*e.g.* earlier reoperation might be suggested in the event of dlPFC, vPMc, or STG infiltration). Second, our results pave the way for future interventional therapies aimed at fostering individual dynamics of plasticity or "meta-plasticity" (a term recently reappraised to account for the susceptibility of brain plasticity to adapt its learning rules in an ever changing context).[61] For example, cortical areas associated with a high potential of continuous plasticity may be potential targets for non-invasive neuromodulation therapy. Such a proactive approach coupled with cognitive stimulation may help accelerate cortical redistributions and thus allows earlier reoperation and greater extent of resection while minimizing the likelihood of postoperative deficits.[62]

Limitations

Our main findings must be interpreted in light of several limitations. First, the cerebral cortex was not uniformly covered by cortical electrostimulations given that the topological distribution of DES sites was conditional to that of tumour (re)infiltration. Second, due to the clinical context of the study, some biological and therapeutical variables with a potential influence on neuroplasticity could not be directly controlled between the two surgeries (*e.g.* time interval between Surg.1 and Surg.2, switch of antiepileptic drugs, use of adjuvant chemotherapy), although adjusted statistical analyses did not suggest critical a determinant effect of these variables on plasticity changes. Third, thirteen patients (12.9%) presented with a shift of their histomolecular grade toward higher-grade gliomas, which may impact our results. In these patients, it is possible that the dynamic potential for cortical reorganization between both surgeries might have been lowered.[16] Fourth, we considered negative stimulation sites as

cortical areas free of function, which is a necessary reductionist (but clinically relevant) approach given the fact that these areas are not stimulated for the large array of existing cognitive and fine-grained motor functions. For example, all aspects of motor control ere not assessed,[63,64] meaning that the neuroplasticity potential of motor regions might have been underestimated. This potential shortcoming is however mitigated by the clinical observation that surgical removal of negative sites is not associated with a postoperative decline of intraoperatively unassessed functions.[19,26] Last, the probability of observing a loss of functional sites at Surg.2 (*i.e.* a functional area at Surg.1 turning negative at Surg.2) was higher than the probability of observing a displacement of positive sites (*i.e.* the migration of one positive stimulation at Surg.1 to another area at Surg.2). This suggests that remote, nonlocal compensatory cortical sites are potentially recruited (either in the ipsilateral or contralateral hemisphere), beyond the cortical surface exposed during surgery which is necessarily limited.

Conclusions

Overall, our findings indicate that the slow re-growth of DLGGs favours a gradual and evolving remodelling of the cerebral cortex from one surgery to another. This dynamic potential can be expressed as a gradient to the extent that some cortical areas (the dorsolateral prefrontal cortex, the ventral premotor cortex, the superior temporal gyrus) display a higher propensity to reorganize than others (primary sensorimotor cortices). Furthermore, the efficiency of cortical reorganization may be domain-specific, with a higher potential for cortical circuits underpinning language and speech production. Taken together, these novel findings provide a new insight into the neuroplastic properties of cortical networks and are of immense interest for the clinical management of patients, especially in case of tumour recurrence.

Funding

No funding was received towards this work.

Competing interests

The authors report no competing interests.

Supplementary material

Supplementary material is available at *Brain* online.

References

1. Mesulam M. From sensation to cognition. *Brain*. 1998;121(6):1013-1052. doi:10.1093/brain/121.6.1013
2. Buonomano DV, Merzenich MM. Cortical plasticity: From Synapses to Maps. *Annu Rev Neurosci*. 1998;21(1):149-186. doi:10.1146/annurev.neuro.21.1.149
3. Sampaio-Baptista C, Johansen-Berg H. White Matter Plasticity in the Adult Brain. *Neuron*. 2017;96(6):1239-1251. doi:10.1016/j.neuron.2017.11.026
4. Li P, Legault J, Litcofsky KA. Neuroplasticity as a function of second language learning: Anatomical changes in the human brain. *Cortex*. 2014;58:301-324. doi:10.1016/j.cortex.2014.05.001
5. Herholz SC, Zatorre RJ. Musical Training as a Framework for Brain Plasticity: Behavior, Function, and Structure. *Neuron*. 2012;76(3):486-502. doi:10.1016/j.neuron.2012.10.011
6. Zatorre RJ, Fields RD, Johansen-Berg H. Plasticity in gray and white: neuroimaging changes in brain structure during learning. *Nat Neurosci*. 2012;15(4):528-536. doi:10.1038/nn.3045
7. Rocha RP, Koçillari L, Suweis S, et al. Recovery of neural dynamics criticality in personalized whole-brain models of stroke. *Nat Commun*. 2022;13(1):3683. doi:10.1038/s41467-022-30892-6
8. Salvalaggio A, De Filippo De Grazia M, Zorzi M, Thiebaut de Schotten M, Corbetta M. Post-stroke deficit prediction from lesion and indirect structural and functional disconnection. *Brain*. 2020;143(7):2173-2188. doi:10.1093/brain/awaa156
9. Stockert A, Wawrzyniak M, Klingbeil J, et al. Dynamics of language reorganization after left temporo-parietal and frontal stroke. *Brain*. 2020;143(3):844-861. doi:10.1093/brain/awaa023

10. Louis DN, Perry A, Wesseling P, et al. The 2021 WHO Classification of Tumors of the Central Nervous System: a summary. *Neuro-Oncology*. 2021;23(8):1231-1251. doi:10.1093/neuonc/noab106

11. Duffau H. Lessons from brain mapping in surgery for low-grade glioma: insights into associations between tumour and brain plasticity. *The Lancet Neurology*. 2005;4(8):476-486. doi:10.1016/S1474-4422(05)70140-X

12. Duffau H. The huge plastic potential of adult brain and the role of connectomics: New insights provided by serial mappings in glioma surgery. *Cortex*. 2014;58:325-337. doi:10.1016/j.cortex.2013.08.005

13. Venkataramani V, Tanev DI, Strahle C, et al. Glutamatergic synaptic input to glioma cells drives brain tumour progression. *Nature*. 2019;573(7775):532-538. doi:10.1038/s41586-019-1564-x

14. Venkatesh HS, Morishita W, Geraghty AC, et al. Electrical and synaptic integration of glioma into neural circuits. *Nature*. 2019;573(7775):539-545. doi:10.1038/s41586-019-1563-y

15. Jung E, Alfonso J, Osswald M, Monyer H, Wick W, Winkler F. Emerging intersections between neuroscience and glioma biology. *Nat Neurosci*. 2019;22(12):1951-1960. doi:10.1038/s41593-019-0540-y

16. Desmurget M, Bonnetblanc F, Duffau H. Contrasting acute and slow-growing lesions: a new door to brain plasticity. *Brain*. 2006;130(4):898-914. doi:10.1093/brain/awl300

17. Almairac F, Deverdun J, Cochereau J, et al. Homotopic redistribution of functional connectivity in insula-centered diffuse low-grade glioma. *NeuroImage: Clinical*. 2021;29:102571. doi:10.1016/j.nicl.2021.102571

18. Ng S, Deverdun, Jeremy, Lemaitre, Anne-Laure, et al. Precuneal gliomas promote behaviorally relevant remodeling of the functional connectome. *J Neurosurg*. Published online 2022. doi:10.3171/2022.9.JNS221723

19. Lemaitre AL, Herbet G, Ng S, Moritz-Gasser S, Duffau H. Cognitive preservation following awake mapping-based neurosurgery for low-grade gliomas: A longitudinal, within-patient design study. *Neuro-Oncology*. 2022;24(5):781-793. doi:10.1093/neuonc/noab275

20. Herbet G, Maheu M, Costi E, Lafargue G, Duffau H. Mapping neuroplastic potential in brain-damaged patients. *Brain*. 2016;139(3):829-844. doi:10.1093/brain/awv394

21. Ramakrishna R, Hebb A, Barber J, Rostomily R, Silbergeld D. Outcomes in Reoperated Low-Grade Gliomas. *Neurosurgery*. 2015;77(2):175-184. doi:10.1227/NEU.0000000000000753

22. Shofty B, Haim O, Costa M, et al. Impact of repeated operations for progressive low-grade gliomas. *European Journal of Surgical Oncology*. 2020;46(12):2331-2337. doi:10.1016/j.ejso.2020.07.013

23. De Witt Hamer PC, Robles SG, Zwinderman AH, Duffau H, Berger MS. Impact of Intraoperative Stimulation Brain Mapping on Glioma Surgery Outcome: A Meta-Analysis. *JCO*. 2012;30(20):2559-2565. doi:10.1200/JCO.2011.38.4818

24. Picart T, Herbet G, Moritz-Gasser S, Duffau H. Iterative Surgical Resections of Diffuse Glioma With Awake Mapping: How to Deal With Cortical Plasticity and Connectomal Constraints? *Neurosurgery*. 2019;85(1):105-116. doi:10.1093/neuros/nyy218

25. Southwell DG, Hervey-Jumper SL, Perry DW, Berger MS. Intraoperative mapping during repeat awake craniotomy reveals the functional plasticity of adult cortex. *JNS*. 2016;124(5):1460-1469. doi:10.3171/2015.5.JNS142833

26. Ng S, Lemaitre AL, Moritz-Gasser S, Herbet G, Duffau H. Recurrent Low-Grade Gliomas: Does Reoperation Affect Neurocognitive Functioning? *Neurosurgery*. 2022;90(2):221-232. doi:10.1227/NEU.0000000000001784

27. Lu J, Zhao Z, Zhang J, et al. Functional maps of direct electrical stimulation-induced speech arrest and anomia: a multicentre retrospective study. *Brain*. 2021;144(8):2541-2553. doi:10.1093/brain/awab125

28. Sarubbo S, Tate M, De Benedictis A, et al. Mapping critical cortical hubs and white matter pathways by direct electrical stimulation: an original functional atlas of the human brain. *NeuroImage*. 2020;205:116237. doi:10.1016/j.neuroimage.2019.116237

29. Tate MC, Herbet G, Moritz-Gasser S, Tate JE, Duffau H. Probabilistic map of critical functional regions of the human cerebral cortex: Broca's area revisited. *Brain*. 2014;137(10):2773-2782. doi:10.1093/brain/awu168

30. Makale MT, McDonald CR, Hattangadi-Gluth JA, Kesari S. Mechanisms of radiotherapy-associated cognitive disability in patients with brain tumours. *Nat Rev Neurol*. 2017;13(1):52-64. doi:10.1038/nrneurol.2016.185

31. Duffau H. New Philosophy, Clinical Pearls, and Methods for Intraoperative Cognition Mapping and Monitoring "à la carte" in Brain Tumor Patients. *Neurosurgery*. Published online January 19, 2021:nyaa363. doi:10.1093/neuros/nyaa363

32. Sanai N, Mirzadeh Z, Berger MS. Functional Outcome after Language Mapping for Glioma Resection. *N Engl J Med*. 2008;358(1):18-27. doi:10.1056/NEJMoa067819

33. Herbet G, Moritz-Gasser S, Duffau H. Electrical stimulation of the dorsolateral prefrontal cortex impairs semantic cognition. *Neurology*. 2018;90(12):e1077-e1084. doi:10.1212/WNL.0000000000005174

34. Moritz-Gasser S, Herbet G, Duffau H. Mapping the connectivity underlying multimodal (verbal and non-verbal) semantic processing: A brain electrostimulation study. *Neuropsychologia*. 2013;51(10):1814-1822. doi:10.1016/j.neuropsychologia.2013.06.007

35. Duffau H, Ng S, Lemaitre AL, Moritz-Gasser S, Herbet G. Constant Multi-Tasking With Time Constraint to Preserve Across-Network Dynamics Throughout Awake Surgery for Low-Grade Glioma: A Necessary Step to Enable Patients Resuming an Active Life. *Front Oncol*. 2022;12:924762. doi:10.3389/fonc.2022.924762

36. Ng S, Moritz-Gasser S, Lemaitre AL, Duffau H, Herbet G. White matter disconnectivity fingerprints causally linked to dissociated forms of alexia. *Commun Biol*. 2021;4(1):1413. doi:10.1038/s42003-021-02943-z

37. Yordanova YN, Cochereau J, Duffau H, Herbet G. Combining resting state functional MRI with intraoperative cortical stimulation to map the mentalizing network. *NeuroImage*. 2019;186:628-636. doi:10.1016/j.neuroimage.2018.11.046

38. Lüders HO, Dinner DS, Morris HH, Wyllie E, Comair YG. Cortical electrical stimulation in humans. The negative motor areas. *Adv Neurol*. 1995;67:115-129.

39. Rech F, Herbet G, Gaudeau Y, et al. A probabilistic map of negative motor areas of the upper limb and face: a brain stimulation study. *Brain*. 2019;142(4):952-965. doi:10.1093/brain/awz021

40. Penfield W, Boldrey E. Somatic Motor and Sensory representation in the Cerebral Cortex of man as studied by Electrical Stimulation. *Brain*. 1937;60(4):389-443. doi:10.1093/brain/60.4.389

41. Metz-Lutz MN, Kremin H, Deloche G, Hannequin D, Ferrand L, Perrier D, et al. Standardisation d'un test de dénomination orale: contrôle des effets de l'âge, du sexe et du niveau de scolarité chez les sujets adultes normaux. Revue de Neuropsychologie 1991; 1(1): 73-95.

42. Nachev P, Coulthard E, Jäger HR, Kennard C, Husain M. Enantiomorphic normalization of focally lesioned brains. *NeuroImage*. 2008;39(3):1215-1226. doi:10.1016/j.neuroimage.2007.10.002

43. Roux A, Lemaitre AL, Deverdun J, Ng S, Duffau H, Herbet G. Combining Electrostimulation With Fiber Tracking to Stratify the Inferior Fronto-Occipital Fasciculus. *Front Neurosci*. 2021;15:683348. doi:10.3389/fnins.2021.683348

44. Morshed RA, Young JS, Gogos AJ, et al. Reducing complication rates for repeat craniotomies in glioma patients: a single-surgeon experience and comparison with the literature. *Acta Neurochir*. 2022;164(2):405-417. doi:10.1007/s00701-021-05067-9

45. Sarubbo S, De Benedictis A, Merler S, et al. Towards a functional atlas of human white matter: Functional Atlas of White Matter. *Hum Brain Mapp*. 2015;36(8):3117-3136. doi:10.1002/hbm.22832

46. Griffis JC, Metcalf NV, Corbetta M, Shulman GL. Lesion Quantification Toolkit: A MATLAB software tool for estimating grey matter damage and white matter disconnections in patients with focal brain lesions. *NeuroImage: Clinical*. 2021;30:102639. doi:10.1016/j.nicl.2021.102639

47. Feldman DE, Brecht M. Map Plasticity in Somatosensory Cortex. *Science*. 2005;310(5749):810-815. doi:10.1126/science.1115807

48. Hartwigsen G, Saur D. Neuroimaging of stroke recovery from aphasia – Insights into plasticity of the human language network. *NeuroImage*. 2019;190:14-31. doi:10.1016/j.neuroimage.2017.11.056

49. Saur D. Dynamics of language reorganization after stroke. *Brain*. 2006;129(6):1371-1384. doi:10.1093/brain/awl090

50. Bulubas L, Sardesh N, Traut T, et al. Motor Cortical Network Plasticity in Patients With Recurrent Brain Tumors. *Front Hum Neurosci*. 2020;14:118. doi:10.3389/fnhum.2020.00118

51. Traut T, Sardesh N, Bulubas L, et al. MEG imaging of recurrent gliomas reveals functional plasticity of hemispheric language specialization. *Hum Brain Mapp*. 2019;40(4):1082-1092. doi:10.1002/hbm.24430

52. Duffau H, Denvil D, Capelle L. Long term reshaping of language, sensory, and motor maps after glioma resection: a new parameter to integrate in the surgical strategy. *J Neurol Neurosurg Psychiatry*. 2002;72(4):511-516. doi:10.1136/jnnp.72.4.511

53. Ius T, Angelini E, Thiebaut de Schotten M, Mandonnet E, Duffau H. Evidence for potentials and limitations of brain plasticity using an atlas of functional resectability of WHO grade II gliomas: Towards a "minimal common brain." *NeuroImage*. 2011;56(3):992-1000. doi:10.1016/j.neuroimage.2011.03.022

54. Schucht P, Ghareeb F, Duffau H. Surgery for low-grade glioma infiltrating the central cerebral region: location as a predictive factor for neurological deficit, epileptological outcome, and quality of life: Clinical article. *JNS*. 2013;119(2):318-323. doi:10.3171/2013.5.JNS122235

55. Rossi M, Viganò L, Puglisi G, et al. Targeting Primary Motor Cortex (M1) Functional Components in M1 Gliomas Enhances Safe Resection and Reveals M1 Plasticity Potentials. *Cancers*. 2021;13(15):3808. doi:10.3390/cancers13153808

56. Nakajima R, Kinoshita M, Nakada M. Motor Functional Reorganization Is Triggered by Tumor Infiltration Into the Primary Motor Area and Repeated Surgery. *Front Hum Neurosci*. 2020;14:327. doi:10.3389/fnhum.2020.00327

57. van Geemen K, Herbet G, Moritz-Gasser S, Duffau H. Limited plastic potential of the left ventral premotor cortex in speech articulation: Evidence From intraoperative awake mapping in glioma patients: Ventral Premotor Cortex and Speech. *Hum Brain Mapp*. 2014;35(4):1587-1596. doi:10.1002/hbm.22275

58. Giampiccolo D, Duffau H. Controversy over the temporal cortical terminations of the left arcuate fasciculus: a reappraisal. *Brain*. 2022;145(4):1242-1256. doi:10.1093/brain/awac057

59. Margulies DS, Ghosh SS, Goulas A, et al. Situating the default-mode network along a principal gradient of macroscale cortical organization. *Proc Natl Acad Sci USA*. 2016;113(44):12574-12579. doi:10.1073/pnas.1608282113

60. Duffau H, Taillandier L. New concepts in the management of diffuse low-grade glioma: Proposal of a multistage and individualized therapeutic approach. *Neuro-Oncology*. Published online August 2, 2014:nou153. doi:10.1093/neuonc/nou153

61. Duffau H. Introducing the concept of brain metaplasticity in glioma: how to reorient the pattern of neural reconfiguration to optimize the therapeutic strategy. *Journal of Neurosurgery*. 2022;136(2):613-617. doi:10.3171/2021.5.JNS211214

62. Ille S, Kelm A, Schroeder A, et al. Navigated repetitive transcranial magnetic stimulation improves the outcome of postsurgical paresis in glioma patients – A randomized, double-blinded trial. *Brain Stimulation*. 2021;14(4):780-787. doi:10.1016/j.brs.2021.04.026

63. Viganò L, Howells H, Fornia L, et al. Negative motor responses to direct electrical stimulation: Behavioral assessment hides different effects on muscles. *Cortex*. 2021;137:194-204. doi:10.1016/j.cortex.2021.01.005

64. Fornia L, Rossi M, Rabuffetti M, et al. Direct Electrical Stimulation of Premotor Areas: Different Effects on Hand Muscle Activity during Object Manipulation. *Cerebral Cortex*. 2020;30(1):391-405. doi:10.1093/cercor/bhz139

Figure legends

Figure 1 Methodological framework for intraoperative stimulation and acquisition of normalized stimulation sites. (**A**) Intraoperative protocol during wide-awake surgery with cognitive monitoring. (**B** and **C**) Illustration of intraoperative cortical mapping at Surg.1 and Surg.2, based on intraoperative photographs and camera recordings. (**D**) Positioning of stimulation sites (Surg.2, left hemisphere) onto a 3-dimensional pial mesh reconstruction normalized in the Montreal Neurological Institute space (BrainVISA/Anatomist software [Version 5.0, CEA I2BM, CATI Neuroimaging, Inserm IFR49, and CNRS, France]). (**E**) Eligible cortical stimulation sites during Surg.1 (485 positive stimulations, 806 negative stimulations) (**F**) Eligible cortical stimulation sites during Surg.2 (351 positive stimulations, 440 negative stimulations). The same colour legends apply for the whole figure. DES: Direct electrostimulation, LH: left hemisphere, RH: right hemisphere, Surg.: Surgery

Figure 2 Voxelwise and parcelwise probability maps. (**A**) Voxelwise positive probability maps (right panel), based on positive and negative stimulation density maps (left panel, here illustrating density maps within the left hemisphere at Surg.1). (**B**) Voxel-wise probabilistic neuroplasticity maps, illustrating the probability to obtain a positive (*i.e.* functional) response during Surg.1 cortical mapping while obtaining a negative (*i.e.* non-functional) response during Surg.2 cortical re-mapping. (**C**) Parcelwise probability results within the left hemisphere, based on the parcels of the Brainnetome atlas (https://atlas.brainnetome.org/bntatlas). (**D**) Significant results of parcelwise positive probability comparisons within the left hemisphere (*Fisher's exact test, FDR-correction)*. (**E**) Parcelwise probability results within the right hemisphere, based on the parcels of the Brainnetome atlas. (**F**) Significant results of parcelwise positive probability comparisons within the right hemisphere. IPL: inferior parietal lobule, MFG: middle frontal gyrus, PrG: precentral gyrus, Stim.: stimulation, Surg.: surgery. , * indicates $p < 0.05$; ** indicates $p < 0.01$; *** indicates $p < 0.001$

Figure 3 Results of clustering analyses by functional response. (**A**) Direct electrostimulation (DES) sites eliciting anomia and paraphasia and their related cluster centroids (orange mark at surgery 1, red mark at surgery 2) within the left hemisphere. The upper left panel indicates the location of DES sites at surgery 1. The bottom left panel indicates the location of DES sites at surgery 2. The right panel indicates cluster centroids at surgery 1 and surgery 2. (**B**) DES sites

eliciting non-verbal semantic disorders and their related cluster centroids (orange mark at surgery 1, red mark at surgery 2) within the right hemisphere. (**C**) DES sites eliciting speech arrest and dysarthria and their related cluster centroids within the left hemisphere. (**D**) DES sites eliciting speech arrest and dysarthria and their related cluster centroids within the right hemisphere. (**E**) DES sites eliciting negative motor responses and their related cluster centroids within the left hemisphere. (**F**) DES sites eliciting negative motor responses and their related cluster centroids within the right hemisphere. (**G**) DES sites eliciting positive motor responses and their related cluster centroids (white mark at surgery 1, black mark at surgery 2) within the left hemisphere. (**H**) DES sites eliciting positive motor responses and their related cluster centroids (white mark at surgery 1, black mark at surgery 2) within the right hemisphere. Significant displacements of cluster centroids are represented with a black arrow. Significant modifications in Montreal Neurological Institute coordinates are illustrated with a * (*t-test, FDR-correction*). Onsets of new clusters at surgery 2 are indicated with a red circle. Disappearances of clusters at surgery 2 are indicated with an orange circle. Surg.: surgery

Figure 4 Comparisons of individual functional cortical maps. (**A**) Overlap of individual cortical areas being stimulated both at surgery 1 and surgery 2. (**B**) Results of comparisons between surgery 1 and surgery 2 functional cortical maps, illustrated as a 1 minus p-value map considering only selected functional responses and (**C**) all intraoperative functional responses. Statistical analyses were computed with a family-wise error (FWE) threshold set at $P < 0.05$. Significant cortical areas are indicated with a white arrow.

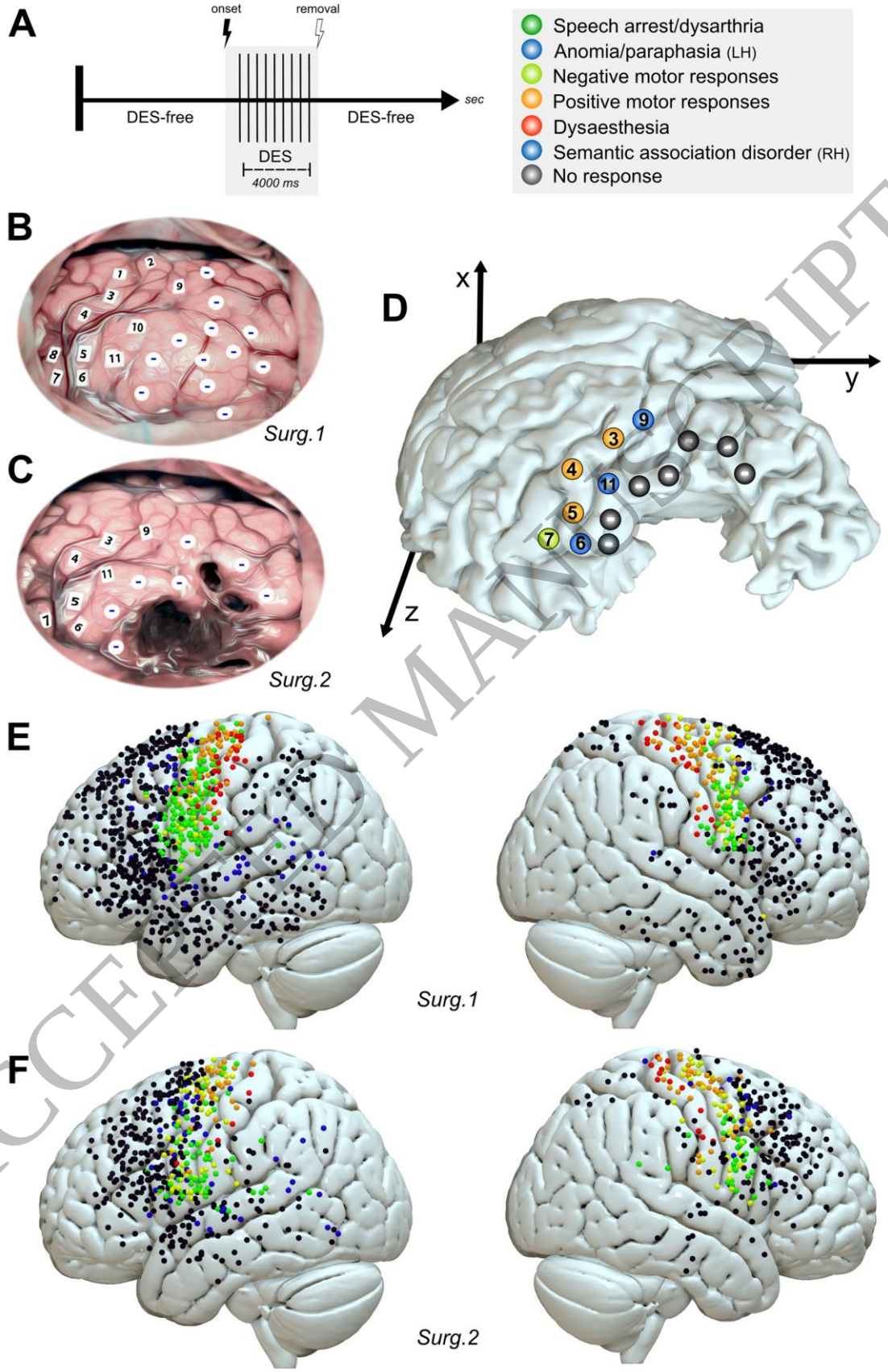

Figure 1
180x263 mm (x DPI)

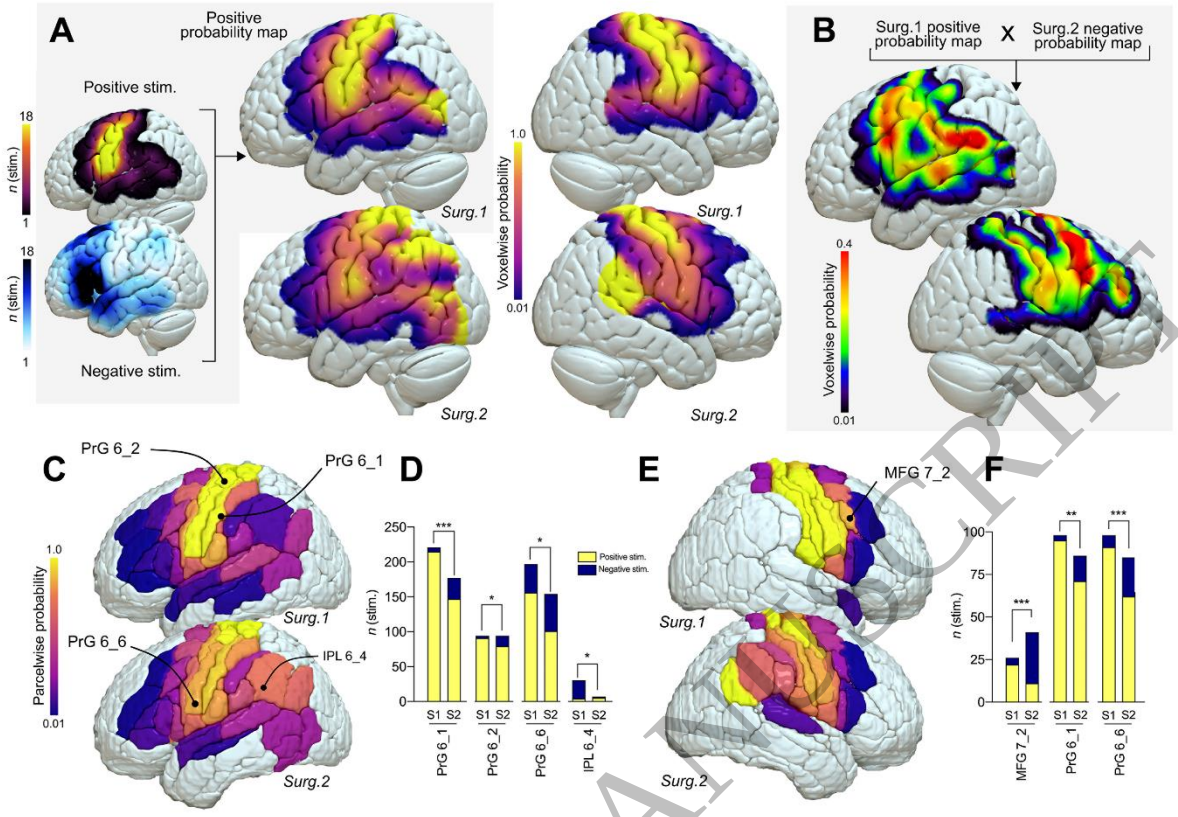

Figure 2
180x124 mm (x DPI)

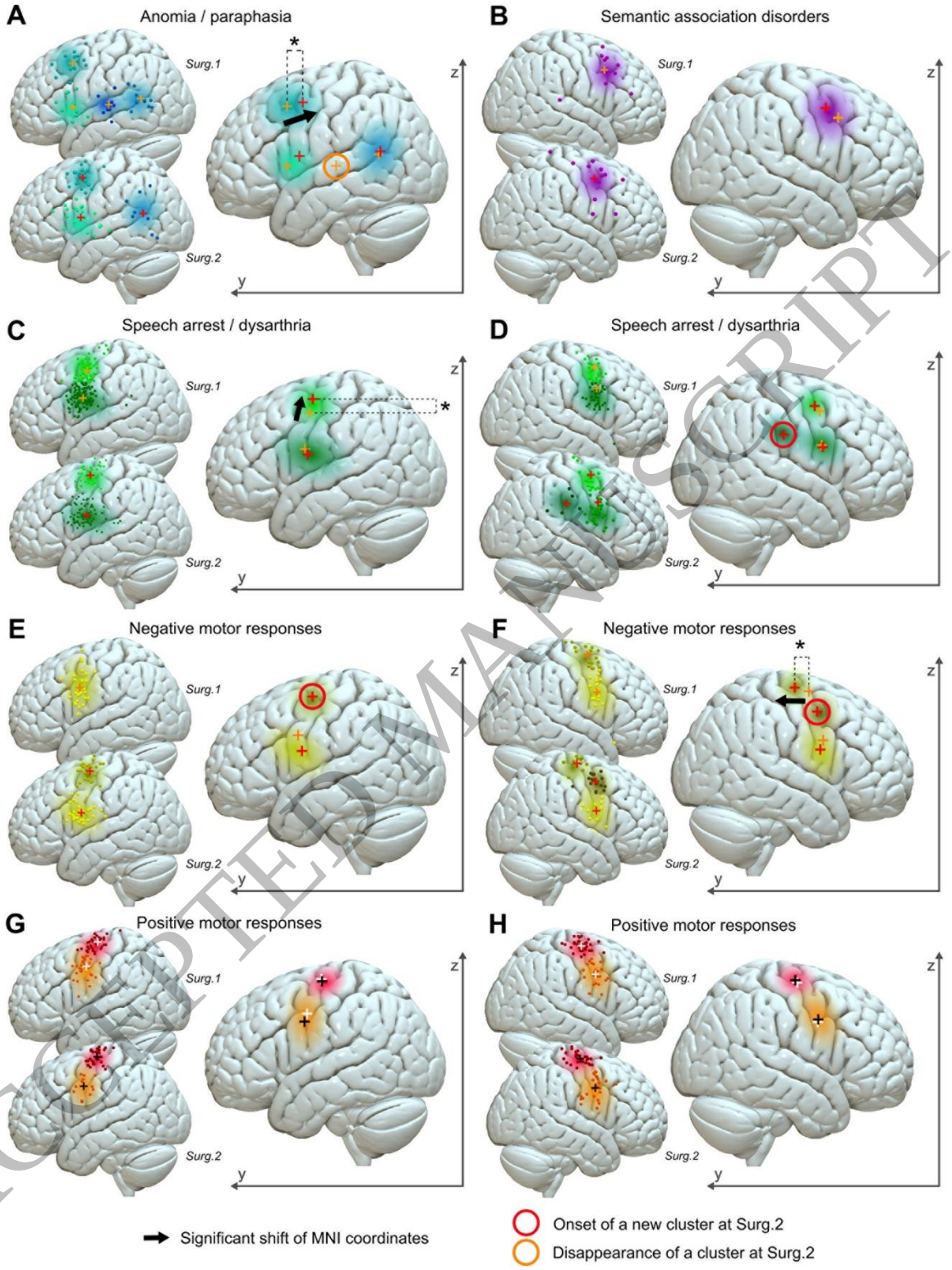

Figure 3
180x233 mm (x DPI)

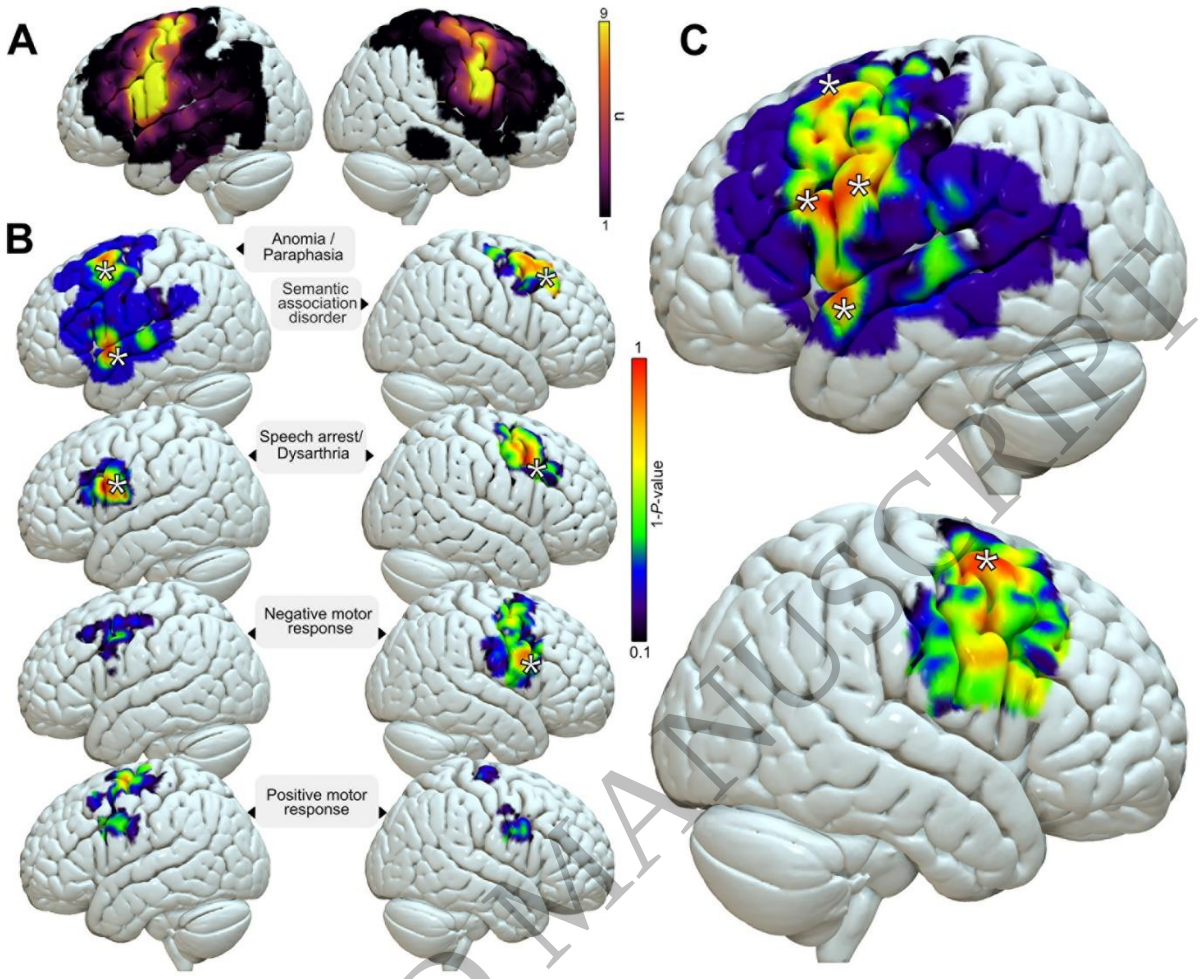

Figure 4
180x152 mm (x DPI)